AGU PUBLICATIONS

JGR

Journal of Geophysical Research: Space Physics

RESEARCH ARTICLE
10.1002/2013JA019646

Key Points:
- Coupling efficiency for HILDCAAs is lower than for CIR and ICME-driven storms
- About 2/3rd of solar wind energy input goes into Joule heating during HILDCAAs
- Joule dissipation during HILDCAAs is larger than that for CIR-storms

Correspondence to:
R. Hajra,
rajkumarhajra@yahoo.co.in

Citation:
Hajra, R., E. Echer, B. T. Tsurutani, and W. D. Gonzalez (2014), Solar wind-magnetosphere energy coupling efficiency and partitioning: HILDCAAs and preceding CIR storms during solar cycle 23, *J. Geophys. Res. Space Physics*, *119*, 2675–2690, doi:10.1002/2013JA019646.

Received 22 NOV 2013
Accepted 26 FEB 2014
Accepted article online 3 MAR 2014
Published online 14 APR 2014
Corrected 16 MAY 2014

This article was corrected on 16 MAY 2014. See the end of the full text for details.

Solar wind-magnetosphere energy coupling efficiency and partitioning: HILDCAAs and preceding CIR storms during solar cycle 23

Rajkumar Hajra[1], Ezequiel Echer[1], Bruce T. Tsurutani[2], and Walter D. Gonzalez[1]

[1]Instituto Nacional de Pesquisas Espaciais (INPE), São José dos Campos, São Paulo, Brazil, [2]Jet Propulsion Laboratory (JPL), California Institute of Technology, Pasadena, California, USA

Abstract A quantitative study on the energetics of the solar wind-magnetosphere-ionosphere system during High-Intensity, Long-Duration, Continuous AE Activity (HILDCAA) events for solar cycle 23 (from 1995 through 2008) is presented. For all HILDCAAs, the average energy transferred to the magnetospheric/ionospheric system was ~6.3×10^{16} J, and the ram kinetic energy of the incident solar wind was ~7.1×10^{18} J. For individual HILDCAA events the coupling efficiency, defined as the ratio of the solar wind energy input to the solar wind kinetic energy, varied between 0.3% and 2.8%, with an average value of ~0.9%. The solar wind coupling efficiency for corotating interaction region (CIR)-driven storms prior to the HILDCAA events was found to vary from ~1% to 5%, with an average value of ~2%. Both of these values are lower than the > 5% coupling efficiency noted for interplanetary coronal mass ejection (and sheath)-driven magnetic storms. During HILDCAAs, ~67% of the solar wind energy input went into Joule heating, ~22% into auroral precipitation, and ~11% into the ring current energy. The CIR-storm Joule heating (~49%) was noticeably less than that during HILDCAAs, while the ring current energies were comparable for the two. Joule dissipation was higher for HILDCAAs that followed CIR-storms (88%) than for isolated HILDCAAs (~60%). Possible physical interpretations for the statistical results obtained in this paper are discussed.

1. Introduction

The aim of this work is to study the solar wind-magnetosphere-ionosphere energetics during High-Intensity, Long-Duration, Continuous AE Activity (HILDCAA) events [*Tsututani and Gonzalez*, 1987] and compare with those of preceding corotating interaction region (CIR)-driven storms (when they occurred). The present study includes events occurring during a period from 1995 through 2008, covering solar cycle (SC) 23.

Both HILDCAAs and CIRs are associated with high-speed (~750–800 km/s) streams (HSSs) emanating from solar coronal holes [*Sheeley et al.*, 1976; *Tsurutani et al.*, 1995]. If the coronal holes last for more than a solar rotation period (~27 days), the corresponding HSSs appear to "corotate" with the Sun, very much like water spewing from a lawn sprinkler. These HSSs, when they interact with slow-speed (~300–400 km/s) streams near the ecliptic plane, give rise to compressed plasma and magnetic field regions, the so-called CIRs [*Smith and Wolfe*, 1976; *Pizzo*, 1985; *Balogh et al.*, 1999]. CIRs are usually formed adjacent to or embedded within the heliospheric current sheet [*Tsurutani et al.*, 1995]. The high plasma densities near the heliospheric current sheet (called the heliospheric plasma sheet) [*Winterhalter et al.*, 1994] and separately, the plasma compressions within the CIR, both cause increases in solar wind ram pressure. Both compress the magnetosphere. These compressions cause gradual storm initial phases prior to the storm main phases [see schematic in *Tsurutani et al.*, 1995]. CIRs, which are characterized by embedded and amplified Alfvén waves, usually lead to weak or moderate geomagnetic storms (Dst > -100 nT: *Tsurutani and Gonzalez* [1997]; *Alves et al.* [2006]). The CIR storms are driven by magnetic reconnection of the southward component of the interplanetary Alfvén waves to the Earth's dayside magnetopause fields. The trailing HSS contains nonlinear Alfvén waves [*Belcher and Davis*, 1971; *Tsurutani et al.*, 1994; *Balogh et al.*, 1995] but lower in amplitude due to the lower field strengths in the HSS proper. These Alfvén waves cause sporadic but continuous magnetic reconnection at the magnetopause, resulting in prolonged periods of geomagnetic activity that can last for days to weeks. The geomagnetic activity has been called HILDCAAs [*Tsurutani and Gonzalez*, 1987; *Tsurutani et al.*, 1995, 2006a, 2006b]. The HSS/HILDCAA interval usually appears as a "recovery phase" of the CIR storm but in actuality is not really a pure recovery as energy is being injected into the magnetosphere throughout the HILDCAA interval.

The orientation of the interplanetary magnetic field (IMF) is the main controlling factor for the solar wind energy transfer into the magnetosphere. The energy transfer is suggested to be a consequence of magnetic reconnection between the southward component of IMF and the Earth's magnetic field [*Dungey*, 1961; *Gonzalez and Mozer*, 1974]. *Gonzalez et al*. [1994] showed that varying amplitudes and durations of IMF polarities may lead to a variable nature of the solar wind-magnetosphere coupling and consequent geomagnetic activities like storms, substorms, and HILDCAAs. For deeper insight into better understanding of the geomagnetic disturbances, detailed qualitative and quantitative studies on the energetics of the events are important. Several case and statistical studies on the energy budget of geomagnetic storms and substorms have been reported previously [e.g., *Weiss et al*., 1992; *Monreal-MacMahon and Gonzalez*, 1997; *Tanskanen et al*., 2002; *Vichare et al*., 2005; *Rosenqvist et al*., 2006; *Turner et al*., 2006, 2009; *de Lucas et al*., 2007; *Guo et al*., 2011, 2012]. However, there have been very few, if any, quantitative studies on the HILDCAA energy budget. According to earlier studies [*Gonzalez et al*., 2006; *Guarnieri*, 2006; *Tsurutani et al*., 2006a], storms and substorms tend to have greater energetic electron fluxes (particle precipitation) in the upper polar atmosphere causing auroras during their intervals. Substorms are more localized in space in the outer magnetosphere and in local time near midnight, whereas storms can include larger regions of auroral emissions in the inner magnetosphere. HILDCAAs, on the other hand, tend to involve not only the auroral zone but a large area of emission in the polar cap as well, although with less intensity than storms [*Guarnieri*, 2006]. These results were based on case studies involving several events using auroral images from the POLAR satellite. Low-level injection of protons into the outer portion of ring current was also reported during HILDCAAs using observations from the low-altitude polar orbiting NOAA 12 satellite [*Søraas et al*., 2004]. These injections were present only at $L > 4$. A quantitative study on the solar wind energy transfer and magnetospheric/ionospheric energy partitioning during HILDCAAs has never been performed to date.

Hajra et al. [2013] studied the long-term variability of HILDCAAs for about 3½ solar cycles (1975–2011). They reported characteristic differences among HILDCAA events occurring during different solar activity phases. In the present work, a quantitative study will be performed on the solar wind-magnetosphere energy coupling and partitioning of the energy during HILDCAA events and their preceding CIR storms (when they occurred) for the first time.

2. Data and Method of Analyses

Recently, *Hajra et al*. [2013] developed a database of HILDCAA events satisfying the four strict "HILDCAA criteria" proposed by *Tsurutani and Gonzalez* [1987]. The criteria are that HILDCAAs have peak AE intensity greater than 1000 nT and last a minimum of 2 days and the high auroral activity continues without the AE value dropping below 200 nT for more than 2 h at a time. Further, the events must occur outside the main phases of geomagnetic storms. We use the *Akasofu* [1981] and *Gonzalez et al*. [1994] definition of a decrease in Dst with peak Dst ≤ -50 nT for a magnetic storm. A total of 133 HILDCAAs were identified during the period 1975–2011 when high-resolution (1 min) AE and Dst data (1 h) were available (see *Hajra et al*. [2013] for a detailed description of event identification). We use all 43 events occurring during 1995 to 2008 (SC 23) for the present study of the HILDCAA energy budget. The outer radiation belt effects associated with the same events have been studied by *Hajra et al*. [2014]. Each HILDCAA event was characterized by four parameters: (i) the time-integrated AE value throughout the event (IAE), (ii) the average AE value during the event ($<$AE$>$), (iii) the peak AE value for the event (AE_p), and (iv) the duration of the event (D).

The HILDCAA events were separated into storm-preceded HILDCAAs (SH) and non-storm or isolated HILDCAAs (H). HILDCAAs starting after the end of storm main phases and well inside the storm recovery phases were defined as SH events. The geomagnetic storms preceding these SH events were driven by CIRs. On the other hand, HILDCAAs not preceded by any storm main phase were identified as H events. Among the 43 events in the study, 32 were H events and 11 were SH events.

We further separated the events according to their occurrence in different solar cycle phases, namely the ascending phase (1998–1999), solar maximum (2000–2002), the descending phase (2003–2005), and solar minimum (1995–1997 and 2006–2008). For statistical studies, we combined the events occurring during the ascending phase and solar maximum and call them AMAX events. We also combined the events occurring during the descending phase and solar minimum and call them DMIN events. The present study involves 11 AMAX events and 32 DMIN events. We formed these two groupings for two reasons. First, it was shown by

Hajra et al. [2013] that the properties of HILDCAAs, like AE intensity and duration, are comparable during the descending phase and solar minimum, and likewise during the ascending phase and solar maximum. DMIN-phase events are > 20% longer in duration that the AMAX-phase events. The second reason is that there is a lack of sufficient number of events to conduct a statistical study if we consider the phases separately. Additional data from other solar cycles would be needed, and this is beyond the scope of the present study.

The solar wind ram kinetic energy budget was computed from the kinetic energy flux per unit time for particles in the interplanetary medium, Usw: $NswVsw^3R_{CF}^2$. In this expression, Vsw and Nsw are the velocity and mass density of the solar wind, respectively. R_{CF} is the Chapman-Ferraro magnetopause distance [*Chapman and Ferraro*, 1931; *Ferraro*, 1952] obtained from the balance between the solar wind kinetic plasma pressure and the magnetospheric magnetic pressure [*Spreiter et al*., 1966; *Holzer and Slavin*, 1979; *Sibeck et al*., 1991; *Monreal-MacMahon and Gonzalez*, 1997; *Shue et al*., 1997; *Shue and Chao*, 2013]. The energy transfer rate from the solar wind to the magnetosphere was determined by the modified Akasofu parameter (ε*): $VswBo^2\sin^4(\theta/2)R_{CF}^2$ [*Perreault and Akasofu*, 1978], where Bo is the IMF magnitude and θ is the clock angle between the geomagnetic field vector and the IMF vector in the equatorial plane. Note that here we have altered the original Akasofu parameter by replacing a fixed magnetosphere scale size by R_{CF}, a solar wind pressure-related term [*Monreal-MacMahon and Gonzalez*, 1997]. The Akasofu expression is based on the consideration of reconnection as the responsible mechanism for the solar wind energy transfer into the magnetosphere.

We estimated separately the rates of energy dissipation via Joule heating (U_J), auroral precipitation (U_A), and ring current injection (U_R). U_J was calculated according to the relations derived by *Knipp et al*. [2004]: $a|PC| + bPC^2 + c|Dst| + dDst^2$, where PC is the polar cap potential index and the constants (a, b, c, and d) depend on the seasons (northern hemispheric). To obtain a global value (for both hemispheres) of U_J, northern hemispheric values were doubled during equinoxes, while the summer estimate was added to the winter estimate for summer and winter months. U_A was computed from NOAA/TIROS satellite measurements of high-latitude precipitating electron and ion fluxes with energies from 50 eV (or 300 eV) to 20 keV (see *Foster et al*. [1986]; *Fuller-Rowell and Evans* [1987]; *Emery et al*. [2006] for details). Global U_A was calculated by adding a southern hemisphere estimate to a northern hemisphere estimate. U_R is of the form: $dDst^*/dt + Dst^*/\tau$ [*Akasofu*, 1981], where Dst* is the modified Dst index after solar wind pressure correction [*Burton et al*., 1975] and removal of induced ground current and magnetotail current effects [*Turner et al*., 2001]. τ is the average ring current decay time, taken as 8 h for the present study [*Yokoyama and Kamide*, 1997; *Guo et al*., 2011]. The total input and dissipation energies, Esw, Eε*, E_J, E_A, and E_R, were calculated by integrating the power terms: Usw, ε*, U_J, U_A, and U_R, respectively, during the entire interval of each storm main phase and HILDCAA event. The total solar wind input energy divided by the total solar wind kinetic energy in percentage gives the coupling efficiency of each HILDCAA interval and CIR storm. Similarly, we estimated the dissipation rates as the percentage of total solar wind input energy. It may be mentioned that the above-described methodology of estimation of magnetospheric/ionospheric energy budget has been being widely used during geomagnetic storms [e.g., *Turner et al*., 2006, 2009; *Guo et al*., 2011, 2012].

The AE (1 min time resolution), Dst (1 h) and SYM-H (1 min time resolution symmetric horizontal component of ring current/Dst) indices were collected from the World Data Center for Geomagnetism, Kyoto, Japan (http://wdc.kugi.kyoto-u.ac.jp/). Descriptions of the indices may be found in *Sugiura* [1964], *Davis and Sugiura* [1966], and *Rostoker* [1972]. Solar wind/interplanetary data at ~1 AU given at 1 min time resolution were obtained from the OMNI website (http://omniweb.gsfc.nasa.gov/). OMNI interplanetary data had been already time adjusted to take into account the solar wind convection time from the spacecraft to the bow shock, so no further adjustments to the interplanetary data were necessary (see http://omniweb.gsfc.nasa.gov/html/omni_min_data.html).

3. Results

3.1. Event Case Studies

Figure 1 shows examples of two HILDCAA events and their corresponding energetics. From top to bottom, the panels show the variations of solar wind kinetic power (Usw), solar wind-magnetosphere coupling function (ε*), ionospheric dissipation power (U_I), ring current injection rate (U_R), IMF Bz, SYM-H, and the AE indices. U_I involves rates of Joule heating (U_J) and auroral particle precipitation (U_A). In the AE panels, the

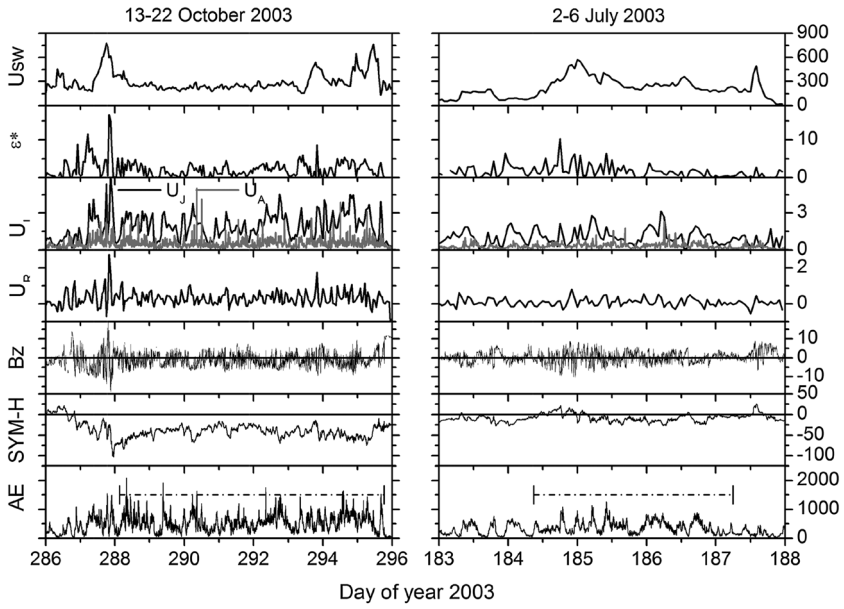

Figure 1. Examples of two High-Intensity, Long-Duration, Continuous AE Activity (HILDCAA) events occurring during (left panel) October 2003 and (right panel) July 2003, and corresponding energetics. From top to bottom, the panels show the variations of solar wind kinetic power (Usw in 10^{11} W), solar wind-magnetosphere energy coupling function (ε^* in 10^{11} W), ionospheric energy dissipation rates (U_J and U_A in 10^{11} W), ring current injection rate (U_R in 10^{11} W), IMF Bz (nT), SYM-H (nT), and the AE (nT) indices. In the AE panels, the horizontal dash-dot lines indicate the intervals of the HILDCAA events. The event on the left panel was preceded by a geomagnetic storm main phase (MP) (peak SYM-H = −103 nT) and occurred in the storm recovery phase, while the event on the right was not preceded by a geomagnetic storm (peak SYM-H = −28 nT).

horizontal dash-dot lines indicate the durations of the HILDCAAs. The event on the left panel was preceded by a CIR-induced storm main phase (peak SYM-H = −103 nT). The July 2003 event on the right panel was not preceded by a geomagnetic storm (peak SYM-H = −28 nT). Both events were associated with large-amplitude fluctuations in IMF Bz. These fluctuations were most likely interplanetary Alfvén waves that have been shown and discussed in many previous works [*Belcher and Davis*, 1971; *Tsurutani et al*., 1982, 1990, 2011a, 2011b; *Tsurutani and Gonzalez*, 1987; *Echer et al*., 2011].

For the SH event during October 2003 (left panel of Figure 1), Usw and ε^* were significantly enhanced during the storm main phase. A peak in the U_R value also occurred during this phase. However, the total (time-integrated) kinetic energy (Esw), solar wind energy input ($E\varepsilon^*$), and dissipation energies (E_J, E_A, E_R) were larger in the HILDCAA interval than in the storm main phase. During the main phase, Esw was ~3.9×10^{18} J, while it was ~19.0×10^{18} J during the following HILDCAA period. During the main phase, $E\varepsilon^*$ available for redistribution in the inner magnetosphere/ionosphere was ~4.9×10^{16} J, ~1.3% of Esw. $E\varepsilon^*$ was ~13.6×10^{16} J, ~0.7% of Esw during HILDCAA interval. Clearly, a larger part of solar wind kinetic energy was available for redistribution in magnetosphere/ionosphere during the main phase of the geomagnetic storm than in the HILDCAA period, although the total available magnetospheric energy during HILDCAA interval was ~3 times of that in the main phase. This indicates larger solar wind-magnetosphere energy coupling efficiency during the main phase of the storm than in the HILDCAA interval. Joule dissipation (E_J) during the storm main phase was ~2.1×10^{16} J, i.e., ~43% of $E\varepsilon^*$. E_J was ~12.0×10^{16} J, ~88% of $E\varepsilon^*$ during the HILDCAA interval. The energy was also found to be dissipated in the auroral ionosphere in the form of auroral particle precipitation during the entire HILDCAA period. An interesting feature is the high-frequency fluctuation in the ionospheric precipitation rates that is characteristic of HILDCAA events. The energies dissipated by the process of ring current injection during the main phase (~9% of $E\varepsilon^*$) and the HILDCAA period (~15% of $E\varepsilon^*$) were significantly smaller than those dissipated by Joule heating.

The right panel of Figure 1 shows that the H event during July 2003 was comparatively shorter and weaker than the SH event. Total solar wind kinetic energy (Esw ~7.1×10^{18} J) and solar wind energy input ($E\varepsilon^*$ ~4.6×10^{16} J) during the entire HILDCAA period were also significantly smaller than the SH event. Joule dissipation

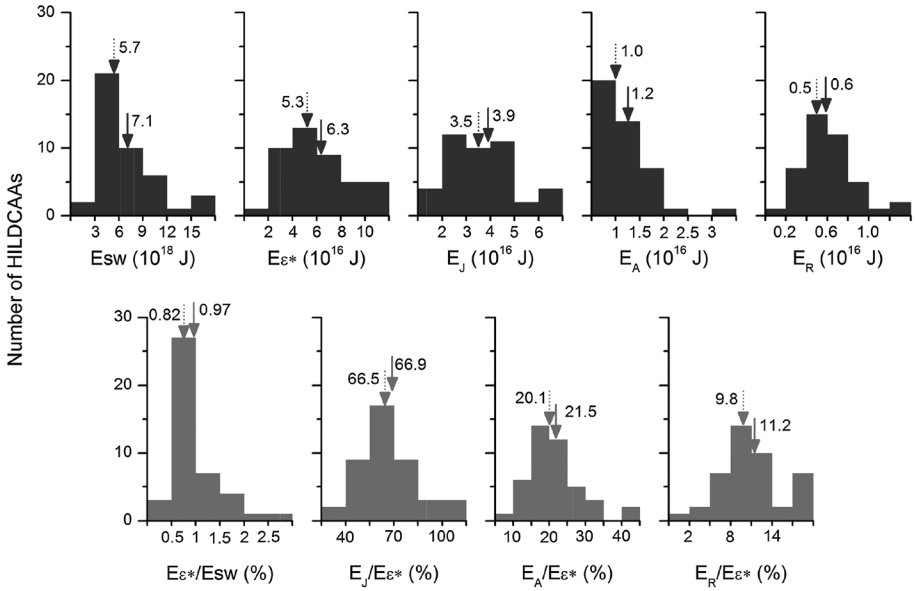

Figure 2. Upper panel: Histograms showing the number of HILDCAA events for different ranges of Esw, Eε*, E_J, E_A, and E_R. Lower panel: Histograms showing number of HILDCAA events for different ranges (%) of Eε*/Esw, E_J/Eε*, E_A/Eε*, and E_R/Eε*. The downward arrows indicate corresponding median (dotted arrow) and mean (solid arrow) values.

was ~2.9×10^{16} J, ~62% of Eε*. The ring current injection (~5% of Eε*) was insignificant compared to the former.

In the following sections, we perform statistical studies on the energy budget of HILDCAA events occurring during SC 23 (1995–2008).

3.2. HILDCAA Energy Budget

The energy budget for all 43 HILDCAA events under study is shown in Figure 2 and summarized in Table 1. The results of the storm main phases (11 events) are also included in Table 1 for comparison. The upper panel of Figure 2 shows the histograms of different energy components involved in the solar wind-magnetosphere-ionosphere system. The entire data set was binned into different energy ranges. All energy components exhibited large variations. The downward pointing arrows indicate the corresponding median (dotted arrow) and mean (solid arrow) values. The solar wind kinetic energy (Esw) during HILDCAAs varied between 2.4×10^{18} and 19.0×10^{18} J with the most typical (mean) value being 7.1×10^{18} J. The solar wind energy input (Eε*) varied between 1.4×10^{16} and 19.3×10^{16} J with an average of 6.3×10^{16} J. A major part of this was dissipated by Joule heating (E_J ~3.9×10^{16} J). The energy injected in the ring current (E_R) varied between 0.1×10^{16} and 2.1×10^{16} J with an average of 0.6×10^{16} J for all events. The average auroral precipitation energy (E_A) was ~1.2×10^{16} J.

The solar wind energy input (Eε*) was compared to the solar wind kinetic energy (Esw) and the dissipation energies (E_J, E_A, and E_R) to the input energy (Eε*) during each event (Table 1 and Figure 2, lower panel). The data set was binned according to different values of the percentage ratios. The lower panel of Figure 2 shows the numbers of events as a function of the percentage ratios. It was observed that between 0.3% and 2.8% of the solar wind kinetic energy was transferred to the magnetosphere during HILDCAA events. On average, Eε* was 0.97% of Esw for all the events.

These values may be compared with those during main phases of CIR storms (Table 1). The 11 storm main phases (preceding the SH events) under study were characterized by peak Dst values varying from −52 to −181 nT with an average value of −89 nT. It was estimated that between 0.8% and 5.4% of the solar wind kinetic energy was transferred to the magnetosphere during the CIR storm main phases. The transfer rate increased linearly (regression coefficient r = 0.86) with the strength (peak Dst) of the storms (not shown), implying stronger solar wind-magnetospheric coupling during the main phases of more intense storms. The

Table 1. HILDCAA (and CIR Storm Main Phase) Energetics[a]

	Average ± SD	Median
	Total energy	
Solar wind Esw (10^{18} J)	7.1 ± 3.9	5.7
	(2.1 ± 1.3)	(1.5)
Magnetosphere Eε* (10^{16} J)	6.3 ± 3.4	5.3
	(4.4 ± 1.9)	(3.0)
Joule heating E_J (10^{16} J)	3.9 ± 1.9	3.5
	(1.6 ± 1.1)	(1.8)
Auroral precipitation E_A (10^{16} J)	1.2 ± 0.6	1.0
	(0.3 ± 0.2)	(0.3)
Ring current E_R (10^{16} J)	0.6 ± 0.3	0.6
	(0.4 ± 0.2)	(0.3)
	Energy transfer/dissipation rate	
Magnetosphere Eε*/Esw (%)	0.97 ± 0.5	0.8
	(2.2 ± 1.8)	(1.3)
Joule heating E_J/Eε* (%)	66.9 ± 19.0	66.5
	(49.0 ± 19.0)	(42.7)
Auroral precipitation E_A/Eε* (%)	21.5 ± 8.0	20.1
	(10.4 ± 4.9)	(13.0)
Ring current E_R/Eε* (%)	11.2 ± 4.7	9.8
	(12.4 ± 5.3)	(11.5)

[a]Total numbers of HILDCAAs and CIR- storm main phases for this analysis are 43 and 11, respectively. The numbers in the parentheses correspond to storm main phases.

average energy transfer rate was 2.2% for all the storm main phases. During the HILDCAA intervals, the average energy transfer rate was about half of that during the main phases of CIR storms.

During HILDCAA events, the largest part of the solar wind energy input was dissipated by Joule heating in the auroral region. The average values of the three dissipation rates were ~67% (Joule heating), 22% (auroral precipitation), and 11% (ring current injection). During the main phases of the preceding CIR storms, ring current injection (~12% of Eε*) was comparable to that during HILDCAAs. However, storm-time Joule heating (49%) and auroral precipitation (10%) were significantly lower compared to those during HILDCAAs.

In Figure 3, the input energy (Eε*) is plotted as a function of solar wind kinetic energy (Esw), and the dissipation energies (E_J, E_A, E_R) are plotted as functions of the input energy during storm main phases (left panel) and HILDCAA events (right panel). The correlation coefficient between Eε* and Esw was far better for the HILDCAA events ($r = 0.69$) than during the main phases of CIR storms ($r = 0.40$). Another interesting result is that, while Joule dissipation was best correlated ($r = 0.81$) with the input energy during the HILDCAAs, ring current injection was best correlated ($r = 0.91$) with the input energy during the storm main phases. It may be mentioned that all the correlation coefficients noted in Figure 3 are statistically significant at a $> 99\%$ confidence level with the exception of that between Eε* and Esw ($r = 0.40$) during storm main phases. The latter was significant at $> 75\%$ confidence level.

3.3. Comparison of Storm-Preceded Events (SH) and Non-Storm Events (H)

The upper panel of Figure 4 shows histograms of HILDCAAs with different ranges of energy. Storm-preceded (SH) and isolated (H) HILDCAAs are shown by different shadings. The average values are marked by downward pointing arrows. The average solar wind kinetic energies (Esw) were comparable for the SH (7.0×10^{18} J) and the H (7.1×10^{18} J) events. The average input energy (Eε*) was larger for the H events (6.5×10^{16} J) than for the SH events (5.4×10^{16} J). However, the average dissipation energies were found to be larger for the SH events than for the H events.

The magnetospheric energy transfer rates and dissipation rates are shown in the lower panel of Figure 4. On average, 1% of solar wind energy was transferred to the magnetosphere during the H events. The amount was 0.87% for the SH events. The dissipation rates were larger during the SH events than during the H events. In both cases, Joule heating was the dominating dissipation mechanism for solar wind energy input. During the SH events, ~88% of input energy was dissipated by Joule heating,

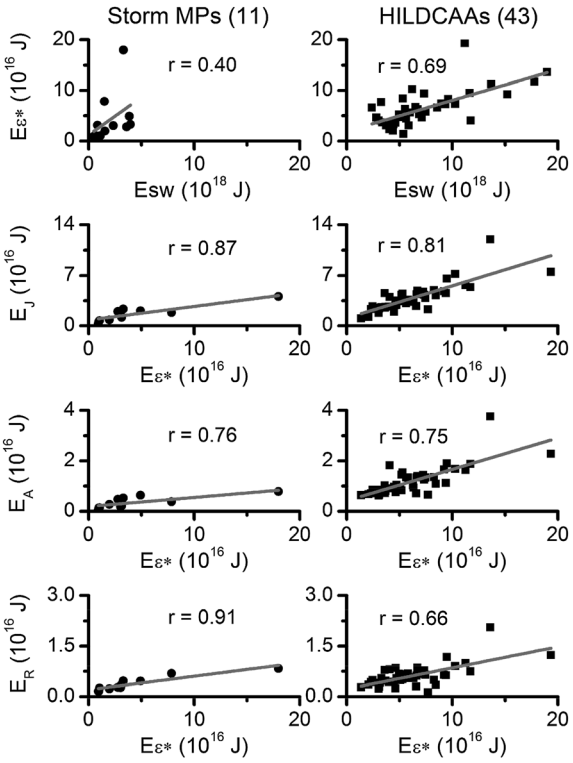

Figure 3. Scatter plots showing the variations of Eε* with Esw, and variations of E_J, E_A, and E_R with Eε*. The left panel pertains to storm main phases (MPs), and the right panel pertains to HILDCAA events. The number of main phases and HILDCAA events is mentioned in the parentheses following the event tags. The linear regression lines and corresponding correlation coefficients (r) are shown in each plot.

while Joule dissipation was ~60% for the H events. The average ring current injection during the SH events (16.2% of Eε*) was ~42% higher than during the H events (9.4% of Eε*). Auroral precipitation was ~27% of Eε* during the SH events and ~20% during the H events, on average. Student's *t*-statistics and the corresponding probability factor p [*Reiff*, 1990] were calculated in order to estimate the statistical significance of the mean dissipation rates. The average dissipation rates of the SH and H events are considered to be significantly different if $p < 0.05$ [*Press et al.*, 1992]. It is observed that the p values for dissipation by Joule heating (E_J/Eε*), auroral precipitation (E_A/Eε*) and ring current injection (E_R/Eε*) are 0.0001, 0.0065, and 0.0001, respectively. Clearly, the fact that the storm-preceded HILDCAAs dissipated larger part of solar wind energy input compared to the isolated HILDCAAs is statistically significant.

Figure 5 shows the energy dissipated into the inner magnetosphere/ionosphere during HILDCAAs (left panel), and the characteristic parameters of HILDCAAs (right panel) as functions of the input energy. The results are compared between the SH and the H events. All the correlation coefficients (shown in the figure) are statistically significant at the > 95%

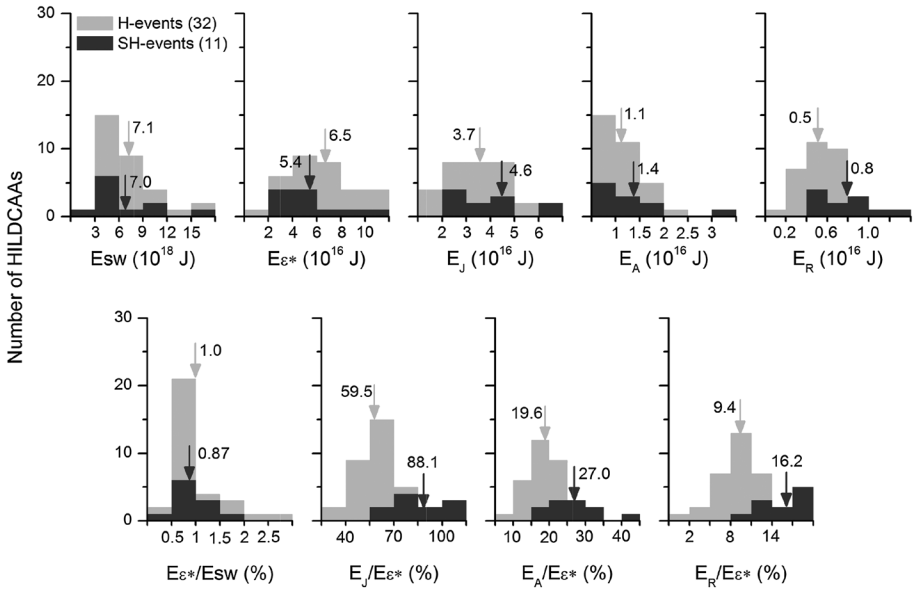

Figure 4. The upper and lower panels are the same as those in Figure 2. The gray and dark gray histograms pertain to non-storm related (H)- and storm-preceded (SH)- HILDCAA events, respectively. The downward arrows indicate the mean values. The numbers of events are given in the parentheses following event legends.

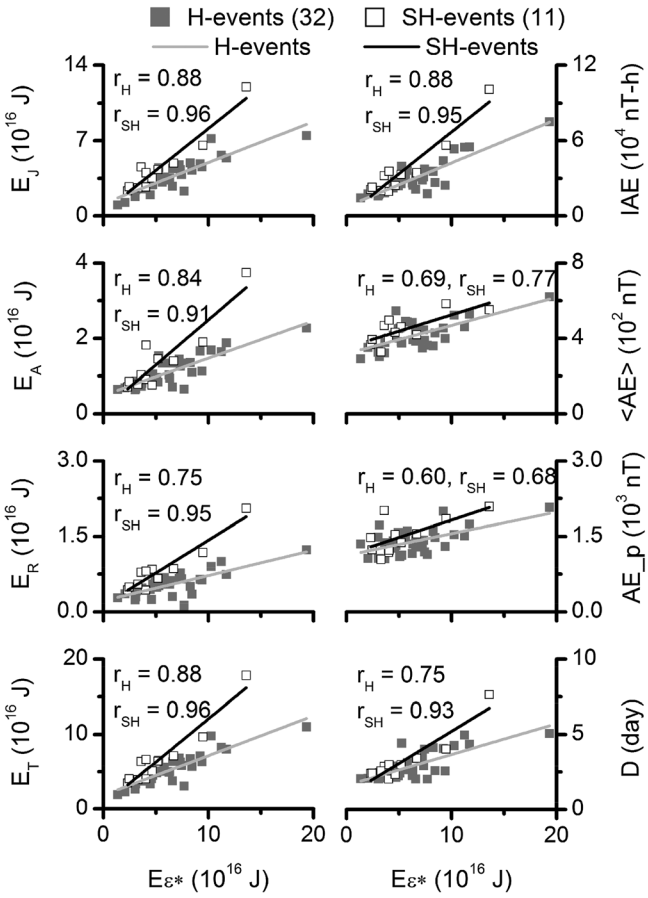

Figure 5. Left panel: Scatter plots showing the variations of E_J, E_A, E_R, and E_T (= $E_J + E_A + E_R$) with Eε*. Right panel: Scatter plots showing the variations of IAE, <AE>, AE_p, and D with Eε*. The filled and open squares show H events and SH events, respectively. The linear regression lines and corresponding correlation coefficients (r) are shown in each plot. The numbers in the parentheses indicate the number of H and SH events.

confidence level. The input energy (Eε*) was best correlated, among the three dissipation mechanisms, with Joule heating for both the SH events (r = 0.96) and the H events (r = 0.88). The overall correlation between dissipation and input energies was higher for the SH events than the H events. Also, the slopes of the linear regression lines were higher for the SH events. These results are consistent with larger dissipation efficiency of the SH events (Figure 4).

The HILDCAA characteristic parameters (IAE, <AE>, AE_p, and D) were found to be well correlated with the magnetospheric energy input (Eε*) during HILDCAAs (right panel, Figure 5). In this case also, the correlation coefficients were higher for the SH events compared to the H events, although the coefficients were statistically significant in both cases. The high and statistically significant correlation coefficients may emphasize the direct solar wind and IMF control on the geomagnetic variations during HILDCAAs or on the HILDCAA energy budget and characteristics.

3.4. Solar Cycle Dependence of HILDCAA Energetics

As mentioned earlier, we combined the events occurring during the solar cycle ascending phase (1998–1999) and solar maximum (2000–2002) of SC 23 and call these AMAX events. We also combined the events occurring during the descending phase (2003–2005) and solar minimum (1995–1997, 2006–2008). These are called DMIN events.

In the upper panel of Figure 6, the histograms of the AMAX and DMIN events are shown for different ranges of solar wind kinetic energy, input energy, and dissipation energies binned by different values.

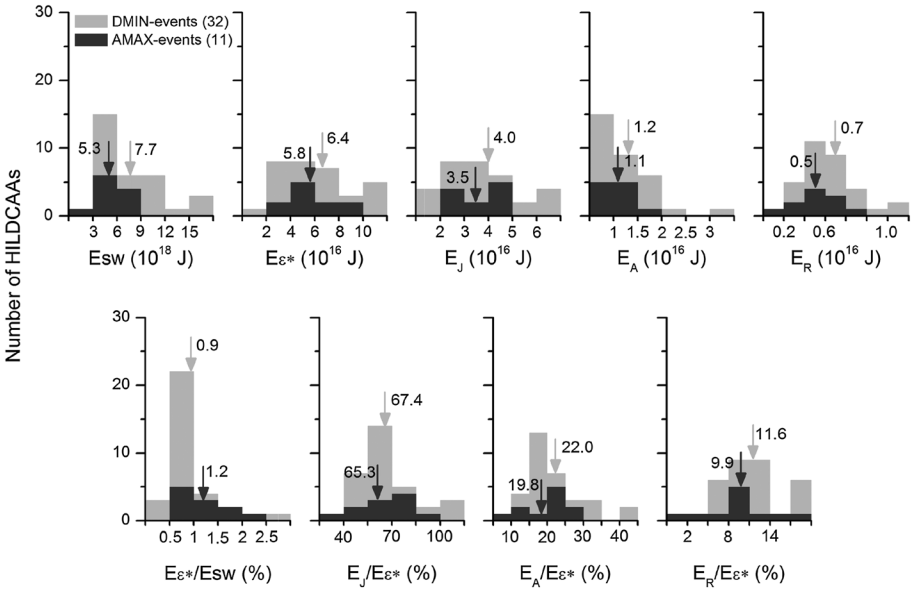

Figure 6. The figure is in the same format as Figure 4, but the gray and dark gray histograms here show the DMIN and AMAX events, respectively.

The average values are shown by downward pointing arrows in each plot. The DMIN events involved, on the average, slightly larger amount of solar wind kinetic energy (Esw ~31% larger), magnetospheric input energy (Eε* ~10% larger), and energies dissipated in the ionosphere (E_J ~14% and E_A ~9% larger) and ring current injection (E_R ~40% larger) than the AMAX events.

The solar wind energy transfer and dissipation rates of magnetospheric energy are compared for the DMIN and AMAX events, shown in the lower panel of Figure 6. While the average rate of solar wind energy transfer was slightly smaller for the DMIN events (0.9%) than for the AMAX events (1.2%), a slightly larger percentage of input energy was dissipated during the DMIN events than the AMAX events. However, as confirmed by Student's *t* test, the dissipation rates bear no statistically distinguishable difference between these two combined phases (AMAX and DMIN).

Figure 7 shows the variations of HILDCAA dissipation energies (left panel) and HILDCAA characteristic parameters (right panel) as functions of the input energy. For the events during the AMAX phases, there was poor or no correlation between the dissipation energies and the input energy. On the other hand, statistically significant correlations (at the $>95\%$ confidence level) were recorded for the events during the DMIN phases. For these events, the correlation of input energy was the highest with Joule energy ($r = 0.83$) compared to the lowest correlation with ring current dissipation ($r = 0.74$). The HILDCAA characteristic parameters exhibited poor or no correlation with the input energy for the AMAX events, while correlations were statistically significant for the DMIN events (right panel, Figure 7).

The difference in the correlation coefficients during the two combined phases (AMAX and DMIN) of the solar cycle is significant. In Figure 8, we plot the percentage distribution of HILDCAAs for different ranges of solar wind speed (Vsw) and IMF Bz during these two phases. We estimated average values of Vsw and Bz during each event. Then the database was binned in different ranges of the average values. The DMIN events exhibited a strong occurrence peak in the high velocity range (550–650 km/s), while for the AMAX events, a strong peak occurred in the lower velocity range ($<$ 500 km/s). From the Bz distribution of the events, it is observed that the DMIN events (~41%) exhibited a stronger peak in the southward Bz sector compared to the AMAX events (~27%). The stronger HSS events and average southward IMF Bz may be responsible for more effective dissipation of energy (geoeffectiveness) in the inner magnetosphere/ionosphere, resulting in better correlation for the DMIN events compared to the AMAX events.

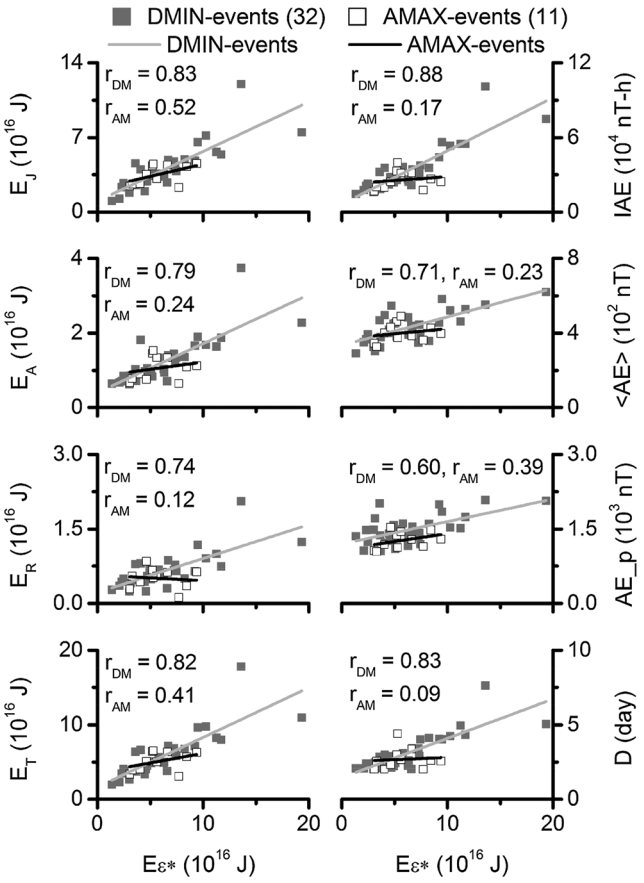

Figure 7. The figure is in the same format as Figure 5, but the filled and open squares here show the DMIN and AMAX events, respectively.

4. Discussion

The solar wind-magnetosphere-ionosphere energy coupling is an important feature of space weather. An accurate measurement of the energy available in the Earth's magnetosphere from the Sun at any given time is not possible. Because of this, many solar wind-magnetosphere coupling functions have been used in the past as proxies [e.g., *Holzer and Slavin*, 1982; *Gonzalez*, 1990; *Stamper et al.*, 1999; *Newell et al.*, 2007; *Tenfjord and Østgaard*, 2013]. We have done the same here. The most widely used parameter for solar wind energy input is the Akasofu (ε*) parameter [*Perreault and Akasofu*, 1978]. Earlier studies, using the ε* parameter, reported that ~5–10% of energy available in the solar wind might be transferred to the magnetosphere during the main phases of geomagnetic storms of varying intensities [e.g., *Weiss et al.*, 1992; *Monreal-MacMahon and Gonzalez*, 1997; *Lu et al.*, 1998; *Østgaard et al.*, 2002; *Vichare et al.*, 2005]. It should be noted that most of the storms studied were large amplitude storms driven by interplanetary coronal mass ejections (ICMEs), the exact drivers being either the upstream sheaths or the magnetic clouds (MCs) within the ICMEs. Our present work involved the energy transfer efficiency study for 11 CIR-driven geomagnetic storms with the peak Dst values varying between −52 nT and −181 nT. For these storm events, the energy input varied from 0.8% to 5.4% of the solar wind kinetic energy. These numbers are lower than those for the ICME storms discussed above. In fact, the range of energy efficiency for CIR storms is about half (~50%) of that for ICME storms.

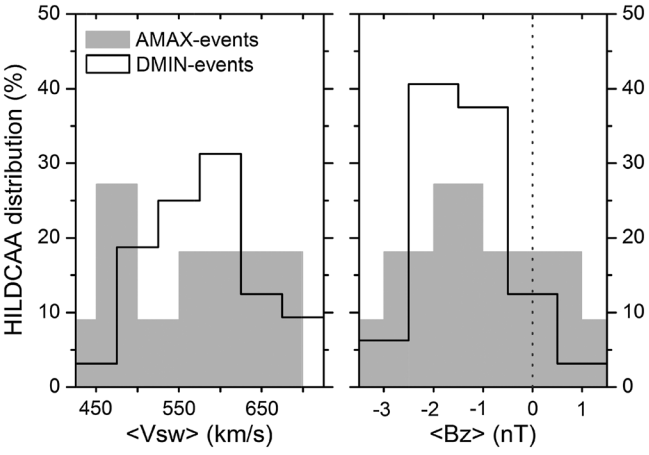

Figure 8. Distributions of HILDCAA events for different ranges of <Vsw> and <Bz>.

Why is the CIR storm energy input efficiency less than ICME storms? The solar wind-magnetosphere energy coupling is controlled by the IMF magnitude, its orientation and the solar wind speed. As mentioned earlier, the energy transfer is suggested to be a consequence of magnetic reconnection between the southward component of IMF and Earth's magnetic field [*Dungey*, 1961; *Gonzalez and Mozer*, 1974]. During the ICME-geomagnetic storm main phases, strong and sustained southward IMF Bz causes effective energy transfer, even when the kinetic energy available in the solar wind is small [*Tsurutani et al.*, 1988; *Monreal-MacMahon and Gonzalez*, 1997]. The

energy coupling is less efficient during CIR storm periods, which is characterized by large fluctuations in Bz between northward and southward directions (Alfvén waves) [*Tsurutani et al*., 1995]. The southward components of Bz are presumably responsible for short reconnection intervals. The magnitude of the southward IMFs in CIRs are typically less than those of MCs (which cause major storms) [*Echer et al*., 2005; *Alves et al*., 2006, 2011].

Why do HILDCAA intervals have lower solar wind coupling efficiencies than do CIR storms? HILDCAA events have solar wind energy transfer rates that varied between 0.3% and 2.8% with an average value of ~1%. The rates are significantly less than even those during the CIR storm main phases. One possible explanation is that the solar wind density and southward IMF amplitude are substantially less in the HSS proper than that in CIRs. Because CIRs are essentially interplanetary sheaths [*Smith and Wolfe*, 1976; *Tsurutani et al*., 1995], the more effective coupling may be attributed to the high plasma densities and stronger IMFs in those structures (compared to HSS proper). However, more effort is needed to verify or deny this hypothesis.

Another important component of the magnetospheric/ionospheric energy budget study is the estimation of energy dissipation in the auroral ionosphere and injection into the ring current (energy partitioning). The relative role of ionospheric Joule heating and ring current injection is an important aspect of many studies. While intense ICME storms appear to dissipate more of the transferred energy in the ring current [*Monreal-MacMahon and Gonzalez*, 1997; *Vichare et al*., 2005], Joule heating dominates as a dissipation channel during the substorm events [e.g., *Østgaard et al*., 2002; *Tanskanen et al*., 2002; *Tenfjord and Østgaard*, 2013, and references therein]. We found that for all HILDCAA events studied, Joule heating accounted for ~2/3rd of the solar wind energy input, while ring current injection was ~1/10th of the input. For the HILDCAA events preceded by the CIR storm main phases or occurring in the storm recovery phases (SH events), Joule dissipation was as large as ~88% of total input energy. The values are consistent with the energy partitioning during CIR-driven storms as reported by *Turner et al*. [2006, 2009]. Our study clearly suggests that Joule heating is the dominant dissipation mechanism during HILDCAA events. A large part of energy was also dissipated in the form of auroral particle precipitation. The ring current injection during HILDCAA events (~11%) and main phases of CIR storms (~12%) was comparable. But the same is considerably less than intense ICME storms. For example, *Monreal-MacMahon and Gonzalez* [1997] reported ring current injection to account for 25% to 40% of the solar wind energy input during the main phases of ICME-driven superstorms (Dst < -240 nT). Lower ring current injection during HILDCAAs may be conceptually understood due to HILDCAAs being driven by short-duration southward IMFs. Not present are the large and long-duration southward IMFs which are the causes of intense ICME storms where the plasma sheet is convected deep into the interior of the magnetosphere near L ~2 [*Tsurutani et al*., 1988; *Gonzalez et al*., 1994].

Present analyses revealed that storm-preceded HILDCAAs (SH) dissipated a larger part of magnetospheric energy in the auroral ionosphere than the non-storm or isolated events (H). A part of the residual storm energy stored in the magnetosphere/magnetotail may contribute during the following auroral activity in case of the SH events [*Du et al*., 2011]. On the other hand, a strong correlation of the energy dissipation and characteristic parameters of the SH events (occurring in the storm recovery phases) with solar wind energy input reinforces the hypothesis that there is fresh input of the solar wind energy in addition to the ring current decay [*Tsurutani et al*., 2004; *Guarnieri*, 2006]. The solar wind and IMF have direct control on the HILDCAA energy budget and on its intensity and duration. More research is needed to understand the characteristic differences between storm-preceded and isolated HILDCAA events.

Another important result of the present study is the strong association of HILDCAA energy dissipation and characteristic parameters with solar wind energy input during the descending and solar minimum phases (DMIN), and lack of correlation during the ascending and solar maximum phases (AMAX). As established by previous works [e.g., *Tsurutani and Gonzalez*, 1987; *Tsurutani et al*., 1990, 1995, 2006a, 2006b], the origin of HILDCAAs lies in magnetic reconnection between the southward components of Alfvén waves (IMF) and Earth's magnetic field. During the DMIN phases, coronal holes extend to lower solar latitudes and expand in size, becoming the dominant solar feature causing geomagnetic activity. HSSs emanate from these coronal holes [*Krieger et al*., 1973; *Sheeley et al*., 1976; *Tsurutani et al*., 1995]. CIRs are formed at the leading edges of the fast streams due to interactions with slow background streams [*Smith and Wolfe*, 1976; *Pizzo*, 1985; *Balogh et al*., 1999]. CIRs, which are characterized by Alfvén waves, usually lead to weak or moderate geomagnetic storms (Dst > -100 nT: *Tsurutani and Gonzalez* [1997]) and the trailing HSS proper causes

prolonged periods of geomagnetic activity [*Tsurutani et al*., 1995, 2006a, 2006b; *Guarnieri et al*., 2006a; *Kozyra et al*., 2006; *Turner et al*., 2006]. The HSS/HILDCAA interval appears as a "recovery phase" of the CIR storm, but in actuality there is fresh input of solar wind energy in addition to the ring current decay. The present results indicate that there is direct control of this fresh solar wind energy input on the HILDCAA energy budget and its characteristics during the DMIN phases.

The HSSs emanating from large, equatorial/low-latitude coronal holes during DMIN phases are more geoeffective. That is, the center of the coronal holes where the peak speeds are ~750 to 800 km/s and the magnetic field variability $\Delta B/Bo$ is ~1 to 2 impinge on the magnetosphere (ΔB being the peak-to-peak amplitude of the transverse magnetic field and Bo is the IMF amplitude) (see *Echer et al*. [2011, 2012]; *Tsurutani et al*. [2011a, 2011b]). These solar wind features cause large energy dissipation and more intense and longer-duration HILDCAA events during these intervals.

On the other hand, no direct IMF and solar wind control on the HILDCAAs was found during the AMAX phases when HSS events are rarer. Events during these phases corresponded to lower average HSS speeds ($Vsw < 500$ km/s) and weaker southward (and northward) IMF Bz. These features have been hypothesized by *Tsurutani et al*. [2011b] as being due to superradial expansion of the solar wind. These two factors may be responsible for weaker energy coupling (geoeffectiveness) and poor correlation of HILDCAA characteristics and energy dissipation with the input energy. These results corroborate the recent findings of *Solomon et al*. [2012]. According to their simulation results, under the condition of southward IMF Bz, magnetosphere-ionosphere coupling increases with increased solar wind speed.

5. Summary

This paper reported, for the first time, a quantitative study on the energetics of the solar wind-magnetosphere system and dissipation throughout the inner magnetosphere during HILDCAA events. The statistical study involved 43 HILDCAAs occurring during the period from 1995 to 2008 that covers a solar cycle (SC 23). The main results may be summarized as follows:

1. During HILDCAA events, the average energy available for redistribution in the magnetospheric/ionospheric system was estimated to be ~6.3×10^{16} J, two orders of magnitude lower than (or ~0.9% of) the solar wind ram kinetic energy (~7.1×10^{18} J). This is lower than the coupling efficiency, defined by the percentage of the solar wind energy input to the solar wind kinetic energy, during main phases of CIR-driven storms (~1% to 5%), which in turn is lower than > 5% coupling efficiency noted for storms driven by ICMEs and their sheaths.
2. During HILDCAAs, ~2/3rd (~67%) of the solar wind energy input was dissipated in the auroral ionosphere in the form of Joule heating. Only ~11% of the energy went into the ring current. Joule heating was found to be the dominating dissipation channel during HILDCAA events.
3. Joule dissipation percentage during main phases of CIR-driven geomagnetic storms (~49%) was significantly lower than during HILDCAAs, while the ring current injection values were comparable for the two. Further, ring current injection during HILDCAAs/CIR storm main phases was about half of the reported value for intense ICME storms.
4. During the HILDCAA events preceded by geomagnetic (CIR) storm main phases (SH events), ~88% of solar wind energy input was dissipated as Joule heating, on average. Joule dissipation was estimated to be significantly lower (~60%) for the isolated or non-storm related HILDCAA events (H).
5. During the solar cycle descending and minimum phases (DMIN), the majority of HILDCAAs occurred when the average solar wind speed (Vsw) was > 550–650 km/s. For these cases, the solar wind energy input exhibited statistically significant correlation with HILDCAA dissipation energy ($r \geq 0.74$). During the ascending and maximum phases (AMAX), most HILDCAAs were associated with average $Vsw < 500$ km/s streams. The correlation with dissipation energy was poor or insignificant for these events.
6. HILDCAAs during DMIN phases involved, on average, slightly larger amount of solar wind kinetic energy, input energy, and energies dissipated in the inner magnetosphere/ionosphere compared to the events occurring during AMAX phases. However, the average energy dissipation bears no statistically distinguishable difference between these two combined phases.

6. Final Comments

This study reported a comparative analysis on the solar wind-magnetosphere energy budget involved during HILDCAAs under varying geomagnetic (storm/non-storm HILDCAAs) and solar activity (ascending-maximum/descending-minimum) conditions. As mentioned earlier, a fully accurate measurement of the energy input into the magnetosphere from the solar wind at any given time is not possible. To estimate the energy transfer from the solar wind to the magnetosphere, we used the most widely used modified Akasofu ε^* parameter which was based on empirical data [*Perreault and Akasofu*, 1978]. It gives a first-order approximation for the magnetospheric energy input and may underestimate the actual value [see *Koskinen and Tanskanen*, 2002]. As observed in the present study and also reported previously [e.g., *Knipp et al*., 1998; *Østgaard et al*., 2002], the ε^* parameter does not always provide enough energy to balance the total dissipation energy in the inner magnetosphere and ionosphere. This indicates that there has to be some other energy transfer mechanism than dayside reconnection. *Tsurutani and Gonzalez* [1995] found that 0.1–0.4% of the solar wind kinetic energy may be injected into the magnetosphere by viscous interaction [*Axford and Hines*, 1961]. Another type of solar wind energy transfer mechanism is cross-field diffusion by resonant wave-particle interactions at the dayside magnetopause [*Sonnerup*, 1980; *Tsurutani et al*., 1981; *Tsurutani and Thorne*, 1982; *Gendrin*, 1983]. By this process, ~0.01% of solar wind kinetic energy may penetrate into the magnetosphere. On the other hand, *Pulkkinen et al*. [2002] have shown that the expression used for U_R may be an overestimation of the ring current injection during the intense storms. These factors may introduce some uncertainties in the energy values/dissipation rates obtained in the present analysis. It is important to note that most of the energy budget studies used the same Akasofu parameter (sometimes with some corrections, as given here) as the measure of magnetospheric input power, although different methods were used to evaluate the energy deposition in the auroral ionosphere. For example, many authors used the AE index to estimate Joule heating and auroral precipitation, as suggested by *Ahn et al*. [1983]. We also tested this methodology (not shown) to note that the main results obtained in the present work remain more or less the same. Thus, this present study involving HILDCAAs for the first time may successfully reveal the comparative picture with the earlier results involving geomagnetic storms and substorms.

It should be noted that the auroral energy deposition in the polar cap indicated by *Guarnieri et al.* [2006b] and *Guarnieri* [2006] have not been captured by the analyses in this study. It has recently been noted by *Huang et al*. [2014] that "the total energy in the ionosphere-thermosphere system is not completely captured either by observation or empirical models." It is possible that this energy is substantial [*Guarnieri*, 2006]. One mechanism for providing such energy is the direct flow of the nonlinear interplanetary Alfvén waves to the polar cap region, a phenomenon which should be maximum during HSSs. It has been shown by *Tsurutani et al*. [2003] that Alfvén waves phase steepen in gradients, heat ions, and electrons via the Ponderomotive Force and dissipate their energy via plasma instabilities and concomitant plasma waves. This mechanism is a natural one to explain ion conics over the polar cap and contribute significantly to the polar wind [*Banks and Holzer*, 1968].

Another note may be mentioned about the use of AE index [*Davis and Sugiura*, 1966] for the identification and characterization of HILDCAA events. The current AE network consists of 12 ground-based magnetometer stations distributed roughly evenly in longitude along the auroral oval region. This may have potential impact of the limited accuracy of AE [e.g., *Rostoker*, 1972]. *Newell and Gjerloev* [2011] used a distribution of more than 100 stations under the SuperMAG project [*Gjerloev*, 2009] to improve the AE index and constructed SuperMAG auroral index termed as SME. Use of the SME index for future studies may be interesting, and we will apply it.

Acknowledgments

The work of RH is financially supported by Fundação de Amparo à Pesquisa do Estado de São Paulo (FAPESP) through post-doctoral research fellowship at INPE. One of the authors (EE) would like to thank to the Brazilian CNPq (301233/2011-0) agency for financial support. Portions of this research were performed at the Jet Propulsion Laboratory, California Institute of Technology under contract with NASA.

Masaki Fujimoto thanks Consuelo Cid and an anonymous reviewer for their assistance in evaluating this paper.

References

Ahn, B. H., S. I. Akasofu, and Y. Kamide (1983), The Joule heat production rate and the particle energy injection rate as a function of the geomagnetic indices AE and AL, *J. Geophys. Res.*, *88*, 6275–6287.

Akasofu, S. I. (1981), Energy coupling between the solar wind and the magnetosphere, *Space Sci. Rev.*, *28*, 121–190.

Alves, M. V., E. Echer, and W. D. Gonzalez (2006), Geoeffectiveness of corotating interaction regions as measured by Dst index, *J. Geophys. Res.*, *111*, A07S05, doi:10.1029/2005JA011379.

Alves, M. V., E. Echer, and W. D. Gonzalez (2011), Geoeffectiveness of solar wind interplanetary magnetic structures, *J. Atmos. Sol. Terr. Phys.*, *73*, 1380–1384.

Axford, W. I., and C. O. Hines (1961), A unifying theory of high-latitude geophysical phenomena and geomagnetic storms, *Canadian J. Phys.*, *39*, 1433–1464.

Balogh, A., E. J. Smith, B. T. Tsurutani, D. J. Southwood, R. J. Forsyth, and T. S. Horbury (1995), The heliospheric magnetic field over the south polar region of the sun, *Science*, *268*, 1007–1010.
Balogh, A., et al. (1999), The solar origin of corotating interaction regions and their formation in the inner heliosphere, *Space Sci. Rev.*, *89*, 141–178.
Banks, P. M., and T. E. Holzer (1968), The polar wind, *J. Geophys. Res.*, *73*, 6846–6854.
Belcher, J. W., and L. Davis Jr. (1971), Large-amplitude Alfvén waves in the interplanetary medium: 2, *J. Geophys. Res.*, *76*, 3534–3563, doi:10.1029/JA076i016p03534.
Burton, R. K., R. L. McPherron, and C. T. Russell (1975), An empirical relationship between interplanetary conditions and Dst, *J. Geophys. Res.*, *80*, 4204–4214.
Chapman, S., and V. C. A. Ferraro (1931), A new theory of magnetic storms, part I, The initial phase, *Terr. Magn. Atmos. Electr.*, *36*, 77–97.
Davis, T. N., and M. Sugiura (1966), Auroral electrojet activity index AE and its universal time variations, *J. Geophys. Res.*, *71*, 785–801, doi:10.1029/JZ071i003p00785.
de Lucas, A., W. D. Gonzalez, E. Echer, F. L. Guarnieri, A. Dal Lago, M. R. da Silva, L. E. A. Vieira, and N. J. Schuch (2007), Energy balance during intense and super-intense magnetic storms using an Akasofu ε parameter corrected by the solar wind dynamic pressure, *J. Atmos. Sol. Terr. Phys.*, *69*, 1851–1863.
Du, A. M., B. T. Tsurutani, and W. Sun (2011), Solar wind energy input during prolonged, intense northward interplanetary magnetic fields: A new coupling function, *J. Geophys. Res.*, *116*, A12215, doi:10.1029/2011JA016718.
Dungey, J. W. (1961), Interplanetary magnetic field and the auroral zones, *Phys. Rev. Lett.*, *6*, 47–48.
Echer, E., M. V. Alves, and W. D. Gonzalez (2005), A statistical study of magnetic cloud parameters and geoeffectiveness, *J. Atmos. Sol. Terr. Phys.*, *67*, 839–852.
Echer, E., B. T. Tsurutani, W. D. Gonzalez, and J. U. Kozyra (2011), High speed stream properties and related geomagnetic activity during the whole heliosphere interval (WHI): 20 March to 16 April 2008, *Sol. Phys.*, *274*, 303–320, doi:10.1007/s11207-011-9739-0.
Echer, E., B. T. Tsurutani, and W. D. Gonzalez (2012), Extremely low geomagnetic activity during the recent deep solar cycle minimum, *Proc. Int. Astron. Union*, *7*, 200–209, doi:10.1017/S174392131200484X.
Emery, B. A., D. S. Evans, M. S. Greer, E. Holeman, K. Kadinsky-Cade, F. J. Rich, and W. Xu (2006), The low energy auroral electron and ion hemispheric power after NOAA and DMSP intersatellite adjustments, *NCAR Scientific and Technical Report*, *470*. [Available at http://cedarweb.hao.ucar.edu/instruments/str470.pdf.]
Ferraro, V. C. A. (1952), On the theory of the first phase of a geomagnetic storm: a new illustrative calculation based on an idealized (plane not cylindrical) model field distribution, *J. Geophys. Res.*, *57*, 15–49, doi:10.1029/JZ057i001p00015.
Foster, J. C., J. M. Holt, R. G. Musgrove, and D. S. Evans (1986), Ionospheric convection associated with discrete levels of particle precipitation, *Geophys. Res. Lett.*, *13*, 656–659.
Fuller-Rowell, T. J., and D. S. Evans (1987), Height-integrated Pedersen and Hall conductivity patterns from the TIROS-NOAA satellite data, *J. Geophys. Res.*, *92*, 7606–7618.
Gendrin, R. (1983), Magnetic turbulence and diffusion processes in the magnetopause boundary layer, *Geophys. Res. Lett.*, *10*, 769–771.
Gjerloev, J. W. (2009), A global ground-based magnetometer initiative, *Eos Trans. AGU*, *90*, 230–231, doi:10.1029/2009EO270002.
Gonzalez, W. D. (1990), A unified view of solar wind-magnetosphere coupling functions, *Planet. Space Sci.*, *38*, 627–632.
Gonzalez, W. D., and F. S. Mozer (1974), A quantitative model for the potential resulting from reconnection with an arbitrary interplanetary magnetic field, *J. Geophys. Res.*, *79*, 4186–4194, doi:10.1029/JA079i028p04186.
Gonzalez, W. D., J. A. Joselyn, Y. Kamide, H. W. Kroehl, G. Rostoker, B. T. Tsurutani, and V. M. Vasyliunas (1994), What is a geomagnetic storm?, *J. Geophys. Res.*, *99*, 5771–5792.
Gonzalez, W. D., F. L. Guarnieri, A. L. C. Gonzalez, E. Echer, M. V. Alves, T. Ogino, and B. T. Tsurutani (2006), Magnetospheric energetics during HILDCAAs, in *Recurrent Magnetic Storms: Corotating Solar Wind Streams*, Geophys. Monogr. Ser., vol. 167, edited by B. T. Tsurutani et al., 175 pp., AGU, Washington, D. C., doi:10.1029/167GM15.
Guarnieri, F. L. (2006), The nature of auroras during high-intensity long-duration continuous AE activity (HILDCAA) events: 1998–2001, in *Recurrent Magnetic Storms*: *Corotating Solar Wind Streams*, Geophys. Monogr. Ser., vol. 167, edited by B. T. Tsurutani et al., 235 pp., AGU, Washington, D. C., doi:10.1029/167GM19.
Guarnieri, F. L., B. T. Tsurutani, W. D. Gonzalez, E. Echer, A. L. C. Gonzalez, M. Grande, and F. Søraas (2006a), ICME and CIR storms with particular emphasis on HILDCAA events, *ILWS Workshop 2006*, Goa.
Guarnieri, F. L., B. T. Tsurutani, W. D. Gonzalez, A. L. C. Gonzalez, M. Grande, F. Soraas, and E. Echer (2006b), ICME and CIR storms with particular emphases on HILDCAA events, in *The Solar Influence on the Heliosphere and Earth's Environment: Recent Progress and Prospects*, edited by N. Gopalswamy and A. Bhattacharya, Quest Publ., 266.
Guo, J., X. Feng, B. A. Emery, J. Zhang, C. Xiang, F. Shen, and W. Song (2011), Energy transfer during intense geomagnetic storms driven by interplanetary coronal mass ejections and their sheath regions, *J. Geophys. Res.*, *116*, A05106, doi:10.1029/2011JA016490.
Guo, J., X. Feng, B. A. Emery, and Y. Wang (2012), Efficiency of solar wind energy coupling to the ionosphere, *J. Geophys. Res.*, *117*, A07303, doi:10.1029/2012JA017627.
Hajra, R., E. Echer, B. T. Tsurutani, and W. D. Gonzalez (2013), Solar cycle dependence of High-Intensity Long-Duration Continuous AE Activity (HILDCAA) events, relativistic electron predictors?, *J. Geophys. Res. Space Physics*, *118*, 5626–5638, doi:10.1002/jgra.50530.
Hajra, R., B. T. Tsurutani, E. Echer, and W. D. Gonzalez (2014), Relativistic electron acceleration during high-intensity long-duration continuous AE activity (HILDCAA) events: Solar cycle phase dependences, *Geophys. Res. Lett.*, *41*, doi:10.1002/2014GL059383.
Holzer, R. E., and J. A. Slavin (1979), A correlative study of magnetic flux transfer in the magnetosphere, *J. Geophys. Res.*, *84*, 2573–2578.
Holzer, R. E., and J. A. Slavin (1982), An evaluation of three predictors of geomagnetic activity, *J. Geophys. Res.*, *87*, 2558–2562.
Huang, C. Y., Y.-J. Su, E. K. Sutton, D. R. Weimer, and R. L. Davidson (2014), Energy coupling during the August 2011 magnetic storm, *J. Geophys. Res. Space Physics*, *119*, doi:10.1002/2013JA019297.
Knipp, D. J., et al. (1998), An overview of the early November 1993 geomagnetic storm, *J. Geophys. Res.*, *103*, 26,197–26,220.
Knipp, D. J., W. K. Tobiska, and B. A. Emery (2004), Direct and indirect thermospheric heating sources for solar cycles 21–23, *Sol. Phys.*, *224*, 495–504.
Koskinen, H. E., and E. I. Tanskanen (2002), Magnetospheric energy budget and the epsilon parameter, *J. Geophys. Res.*, *107*(A11), 1415, doi:10.1029/2002JA009283.
Kozyra, J. U., et al. (2006), Response of the upper/middle atmosphere to coronal holes and powerful high-speed solar wind streams in 2003, in *Recurrent Magnetic Storms: Corotating Solar Wind Streams*, Geophys. Monogr. Ser., vol. 167, edited by B. T. Tsurutani et al., 319 pp., AGU, Washington, D. C., doi:10.1029/167GM24.

Krieger, A. S., A. F. Timothy, and E. C. Roelof (1973), A coronal hole and its identification as the source of a high velocity solar wind stream, *Sol. Phys.*, *29*, 505–525.
Lu, G., et al. (1998), Global energy deposition during the January 1997 magnetic cloud event, *J. Geophys. Res.*, *103*, 11,685–11,694.
Monreal-MacMahon, R., and W. D. Gonzalez (1997), Energetics during the main phase of geomagnetic superstorms, *J. Geophys. Res.*, *102*, 14,199–14,207.
Newell, P. T., and J. W. Gjerloev (2011), Evaluation of SuperMAG auroral electrojet indices as indicators of substorms and auroral power, *J. Geophys. Res.*, *116*, A12211, doi:10.1029/2011JA016779.
Newell, P. T., T. Sotirelis, K. Liou, C. I. Meng, and F. J. Rich (2007), A nearly universal solar wind-magnetosphere coupling function inferred from 10 magnetospheric state variables, *J. Geophys. Res.*, *112*, A01206, doi:10.1029/2006JA012015.
Østgaard, N., G. Germany, J. Stadsnes, and R. R. Vondrak (2002), Energy analysis of substorms based on remote sensing techniques, solar wind measurements, and geomagnetic indices, *J. Geophys. Res.*, *107*(A9), 1233, doi:10.1029/2001JA002002.
Perreault, P., and S. I. Akasofu (1978), A study of geomagnetic storms, *Geophys. J. R. Astron. Soc.*, *54*, 547–583.
Pizzo, V. J. (1985), Interplanetary shocks on the large scale: a retrospective on the last decade's theoretical effects, in *Collisionless Shocks in the Heliosphere: Reviews of Current Research*, Geophys. Monogr. Ser., vol. 35, edited by B. T. Tsurutani and R. G. Stone, 51 pp., AGU, Washington, D. C., doi:10.1029/GM035p0051.
Press, W. H., S. A. Teukolsky, W. T. Vetterling, and B. P. Flannery (1992), *Numerical Recipes: The Art of Scientific Computing*, 2nd ed., Cambridge Univ. Press, New York.
Pulkkinen, T. I., N. Y. Ganushkina, E. I. Kallio, G. Lu, D. N. Baker, N. E. Turner, T. A. Fritz, J. F. Fennell, and J. Roeder (2002), Energy dissipation during a geomagnetic storm: May 1998, *Adv. Space Res.*, *30*, 2231–2240.
Reiff, P. H. (1990), The use and misuse of statistics in space physics, *J. Geomagn. Geoelectr.*, *42*, 1145–1174.
Rosenqvist, L., S. Buchert, H. Opgenoorth, A. Vaivads, and G. Lu (2006), Magnetospheric energy budget during huge geomagnetic activity using Cluster and ground-based data, *J. Geeophys. Res.*, *111*, A10211, doi:10.1029/2006JA011608.
Rostoker, G. (1972), Geomagnetic indices, *Rev. Geophys.*, *10*, 935–950, doi:10.1029/RG010i004p00935.
Sheeley, N. R., Jr., J. W. Harvey, and W. C. Feldman (1976), Coronal holes, solar wind streams and recurrent geomagnetic disturbances: 1973–1976, *Sol. Phys.*, *49*, 271–278.
Shue, J. H., and J. K. Chao (2013), The role of enhanced thermal pressure in the earthward motion of the Earth's magnetopause, *J. Geophys. Res. Space Physics*, *118*, 3017–3026, doi:10.1002/jgra.50290.
Shue, J. H., J. K. Chao, H. C. Fu, C. T. Russell, P. Song, K. K. Khurana, and H. J. Singer (1997), A new functional form to study the solar wind control of the magnetopause size and shape, *J. Geophys. Res.*, *102*, 9497–9511.
Sibeck, D. G., R. E. Lopez, and E. C. Roelof (1991), Solar wind control of the magnetopause shape, location and motion, *J. Geophys. Res.*, *96*, 5489–5495.
Smith, E. J., and J. H. Wolfe (1976), Observations of interaction regions and corotating shocks between one and five AU: Pioneers 10 and 11, *Geophys. Res. Lett.*, *3*, 137–140, doi:10.1029/GL003i003p00137.
Solomon, S. C., A. G. Burns, B. A. Emery, M. G. Mlynczak, L. Qian, W. Wang, D. R. Weimer, and M. Wiltberger (2012), Modeling studies of the impact of high-speed streams and corotating interaction regions on the thermosphere-ionosphere, *J. Geophys. Res.*, *117*, A00L11, doi:10.1029/2011JA017417.
Sonnerup, B. U. D. (1980), Theory of the low latitude boundary layer, *J. Geophys. Res.*, *85*, 2017–2026.
Søraas, F., K. Aarsnes, K. Oksavik, M. I. Sandanger, D. S. Evans, and M. S. Greer (2004), Evidence for particle injection as the cause of Dst reduction during HILDCAA events, *J. Atmos. Sol. Terr. Phys.*, *66*, 177–186.
Spreiter, J. R., A. L. Summers, and A. Y. Alksne (1966), Hydromagnetic flow around the magnetosphere, *Planet. Space Sci.*, *14*, 223–253.
Stamper, R., M. Lockwood, M. Wild, and T. D. G. Clark (1999), Solar causes of the long-term increase in geomagnetic activity, *J. Geophys. Res.*, *104*, 28,325–28,342.
Sugiura, M. (1964), Hourly values of Equatorial Dst for the IGY, in *Annual International Geophysical Year*, vol. 35, 9 pp., Pergamon, New York.
Tanskanen, E., T. I. Pulkkinen, H. E. J. Koskinen, and J. A. Slavin (2002), Substorm energy budget during low and high solar activity: 1997 and 1999 compared, *J. Geophys. Res.*, *107*(A6), 1086, doi:10.1029/2001JA900153.
Tenfjord, P., and N. Østgaard (2013), Energy transfer and flow in the solar wind-magnetosphere-ionosphere system: A new coupling function, *J. Geophys. Res. Space Physics*, *118*, 5659–5672, doi:10.1002/jgra.50545.
Tsurutani, B. T., and R. M. Thorne (1982), Diffusion processes in the magnetopause boundary layer, *Geophys. Res. Lett.*, *9*, 1247–1250.
Tsurutani, B. T. and W. D. Gonzalez (1987), The cause of high-intensity long-duration continuous AE activity (HILDCAAs): interplanetary Alfvén wave trains, *Planet. Space Sci.*, *35*, 405–412.
Tsurutani, B. T., and W. D. Gonzalez (1995), The efficiency of "viscous interaction" between the solar wind and the magnetosphere during intense northward IMF events, *Geophys. Res. Lett.*, *22*, 663–666.
Tsurutani, B. T., and W. D. Gonzalez (1997), The interplanetary causes of magnetic storms: a review, in *Magnetic Storms*, Geophys. Monogr. Ser., vol. 98, edited by B. T. Tsurutani et al., 77 pp., AGU, Washington, D. C., doi:10.1029/GM098p0077.
Tsurutani, B. T., E. J. Smith, R. M. Thorne, R. R. Anderson, D. A. Gurnett, G. K. Parks, C. S. Lin, and C. T. Russell (1981), Wave particle interactions at the magnetopause: contributions to the dayside aurora, *Geophys. Res. Lett.*, *8*, 183–186.
Tsurutani, B. T., E. J. Smith, R. R. Anderson, K. W. Ogilvie, J. D. Scudder, D. N. Baker, and S. J. Bame (1982), Lion roars and nonoscillatory drift mirror waves in the magnetosheath, *J. Geophys. Res.*, *87*, 6060–6072, doi:10.1029/JA087iA08p06060.
Tsurutani, B. T., W. D. Gonzalez, F. Tang, S. I. Akasofu, and E. J. Smith (1988), Origin of interplanetary southward magnetic fields responsible for major magnetic storms near solar maximum (1978–1979), *J. Geophys. Res.*, *93*, 8519–8531, doi:10.1029/JA093iA08p08519.
Tsurutani, B. T., T. Gould, B. E. Goldstein, W. D. Gonzalez, and M. Sugiura (1990), Interplanetary Alfvén waves and auroral (substorm) activity: IMP 8, *J. Geophys. Res.*, *95*, 2241–2252, doi:10.1029/JA095iA03p02241.
Tsurutani, B. T., C. M. Ho, E. J. Smith, M. Neugebauer, B. E. Goldstein, J. S. Mok, J. K. Arballo, A. Balogh, D. J. Southwood, and W. C. Feldman (1994), The relationship between interplanetary discontinuities and Alfvén waves: Ulysses observations, *Geophys. Res. Lett.*, *21*, 2267–2270.
Tsurutani, B. T., W. D. Gonzalez, A. L. C. Gonzalez, F. Tang, J. K. Arballo, and M. Okada (1995), Interplanetary origin of geomagnetic activity in the declining phase of the solar cycle, *J. Geophys. Res.*, *100*, 21,717–21,733, doi:10.1029/95JA01476.
Tsurutani, B. T., B. Dasgupta, J. K. Arballo, G. S. Lakhina, and J. S. Pickett (2003), Magnetic field turbulence, electron heating, magnetic holes, proton cyclotron waves, and the onsets of bipolar pulse (electron hole) events: A possible unifying scenario, *Nonl. Proc. Geophys.*, *21*, 27–35.
Tsurutani, B. T., W. D. Gonzalez, F. L. Gonzalez, Y. Kamide, X. Zhou, and J. K. Arballo (2004), Are high-intensity long-duration continuous AE activity (HILDCAA) events substorm expansion events?, *J. Atmos. Sol. Terr. Phys.*, *66*, 167–176.
Tsurutani, B. T., et al. (2006a), Corotating solar wind streams and recurrent geomagnetic activity: A review, *J. Geophys. Res.*, *111*, A07S01, doi:10.1029/2005JA011273.

Tsurutani, B. T., R. L. McPherron, W. D. Gonzalez, G. Lu, N. Gopalswamy, and F. L. Guarnieri (2006b), Magnetic storms caused by corotating solar wind streams, in *Recurrent Magnetic Storms: Corotating Solar Wind Streams*, Geophys. Monogr. Ser., vol. 167, edited by B. T. Tsurutani et al., 1 pp., AGU, Washington, D. C., doi:10.1029/167GM03.

Tsurutani, B. T., E. Echer, F. L. Guarnieri, and W. D. Gonzalez (2011a), The properties of two solar wind high speed streams and related geomagnetic activity during the declining phase of solar cycle 23, *J. Atmos. Sol. Terr. Phys.*, *73*, 164–177.

Tsurutani, B. T., E. Echer, and W. D. Gonzalez (2011b), The solar and interplanetary causes of the recent minimum in geomagnetic activity (MGA23): A combination of midlatitude small coronal holes, low IMF Bz variance, low solar wind speeds and low solar magnetic fields, *Ann. Geophys.*, *29*, 839–849.

Turner, N. E., D. N. Baker, T. I. Pulkkinen, J. L. Roeder, J. F. Fennell, and V. K. Jordanova (2001), Energy content in the storm time ring current, *J. Geophys. Res.*, *106*, 19,149–19,156.

Turner, N. E., E. J. Mitchell, D. J. Knipp, and B. A. Emery (2006), Energetics of magnetic storms driven by corotating interaction regions: A study of geoeffectiveness, in *Recurrent Magnetic Storms: Corotating Solar Wind Streams*, Geophys. Monogr. Ser., vol. 167, edited by B. T. Tsurutani et al., 113 pp., AGU, Washington, D. C., doi:10.1029/167GM11.

Turner, N. E., W. D. Cramer, S. K. Earles, and B. A. Emery (2009), Geoefficiency and energy partitioning in CIR-driven and CME-driven storms, *J. Atmos. Sol. Terr. Phys.*, *71*, 1023–1031.

Vichare, G., S. Alex, and G. S. Lakhina (2005), Some characteristics of intense geomagnetic storms and their energy budget, *J. Geophys. Res.*, *110*, A03204, doi:10.1029/2004JA010418.

Weiss, L. A., P. H. Reiff, J. J. Moses, and B. D. Moore (1992), Energy dissipation in substorms, in *Proceedings of the International Conference on Substorms ICS-1*, Eur. Space Agency Spec. Publ, vol. *ESA-SP-335*, pp. 309–319, European Space Agency, Paris, France.

Winterhalter, D., E. J. Smith, M. E. Burton, N. Murphy, and D. J. McComas (1994), The heliospheric plasma sheet, *J. Geophys. Res.*, *99*, 6667–6680.

Yokoyama, N., and Y. Kamide (1997), Statistical nature of geomagnetic storms, *J. Geophys. Res.*, *102*, 14,215–14,222.

Erratum

In the originally published version of this article, several instances of text were incorrectly typeset. The following have since been corrected and this version may be considered the authoritative version of record.

In the abstract, ~6.3 ×1016 J was changed to ~6.3×10^{16} J.
In the abstract, ~7.1 ×1018 J was changed to ~7.1×10^{18} J.
In section 2, intervals was changed to interval.
In section 3.3, dissipations was changed to dissipation.
In the reference section, Tsurutani et al. (1981) was updated to correct a co-author's name.